Hindawi
Advances in Materials Science and Engineering
Volume 2018, Article ID 2959827, 13 pages
https://doi.org/10.1155/2018/2959827

Research Article

Study on the Bond-Slip Performance of CFSSTs Based on Push-Out Tests

Lai Wang[1,2], **Haitao Chen**[1,2], **Jitao Zhong**[1,2], **Huirong Chen**[1,2], **Wei Xuan**[1,2], **Shuai Mi**[1,2] and **Hongyan Yang**[3]

[1]*Shandong Provincial Key Laboratory of Civil Engineering Disaster Prevention and Mitigation, Shandong University of Science and Technology, Qingdao 266590, China*
[2]*Shandong University of Science and Technology, College of Civil Engineering and Architecture, Qingdao 266590, China*
[3]*Qingdao ENN Jiaocheng Gas Co., Ltd., Qingdao 266300, China*

Correspondence should be addressed to Haitao Chen; skdtjxycht@sdust.edu.cn

Received 10 August 2017; Revised 27 October 2017; Accepted 9 November 2017; Published 11 February 2018

Academic Editor: Enzo Martinelli

To study the interfacial bond-slip performance of concrete-filled square steel tubes (CFSSTs), taking the core concrete strength, slenderness ratio, and width-to-thickness ratio as the influencing factors; 9 specimens were designed with 3 factors and 3 levels for the orthogonal test method. In addition, different from the above 9 specimens, one specimen without rust removal was designed for the purpose of comparison. Based on the bond stress distribution and deformation coordination relationships between the specimens during the push-out tests, a theoretical formula for calculating the relative slip of a CFSST was deduced. The results show that with the increase of load, the relative slip at the loading ends was earlier than that at the free ends of the specimens; the interfacial bond failure and relative slip gradually developed from the two ends towards the centre of the specimens; the increase of the bond stress in the middle part was faster than that at the ends of the specimens. The order of these factors from main to secondary is the presence of rust in the inner wall of the square steel tube, the slenderness ratio, the core concrete strength, and the width-to-thickness ratio.

1. Introduction

CFST (concrete-filled steel tube) structures have the advantages of a high bearing capacity, good plasticity and toughness, convenient construction, and good economic benefits [1, 2]. As an excellent structure, CFST takes full advantage of the interaction and synergy between the steel tube and concrete in the course of loading. Due to the differences in material properties of the steel tube and core concrete, their strains are not completely continuous under the action of load. There is a certain slippage and bond strength between the steel tube and the core concrete. The cooperation between the composition of the steel tube and the core concrete in the CFST is the fundamental reason for this series of advantages, and the bond strength between the steel tube and core concrete directly affects the ability of the two kinds of materials to work together [3–5]. In practical engineering, the bond-slip between the steel tube and core concrete has an important influence on the mechanical behaviour, failure mode, and working performance of the CFST [6]. At the joint of the concrete-filled steel tubular column and steel beam, the load usually acts on the steel tube of the concrete-filled steel tubular column. Through the interfacial bond force or shear connectors, a part of the load is transmitted to the core concrete. Within a certain range of the interfacial bond-slip, the steel tube has the same strain as the core concrete, and both materials can work together. The bond force between the steel tube and core concrete is mainly composed of three parts: chemical bonding action, frictional resistance, and mechanical interlocking action between the steel tube and core concrete [7–9].

Virdi and Dowling [10, 11] have adopted the method of push-out tests to study the bond-slip behaviour of CFSTs.

The test results show that the strength of the core concrete does not clearly influence the bond strength of CFSTs. The trend of the interfacial bond strength is not obvious with the variation in the diameter-to-thickness ratios of the circular steel tubes, and the dispersion of the experimental results is relatively large. However, the interfacial bond strength increased with the increase of the slenderness ratio. The results of the study by Lihong and Shaohuai [12, 13] and Qu et al. [14] show that the strength of the core concrete clearly influences the interfacial bond strength, and the interfacial bond strength increases with the increase of the core concrete strength. In addition, the relation between the bond strength and concrete strength was deduced. The rougher the inner surface of the steel tube is, the higher the bond strength is, and the interface length does not influence the bond strength of CFSTs. Xiushu et al. [15], Yongjian and Jianjun [16], and Chen et al. [17] determine through reciprocating push-out tests on CFST specimens that the bond stress distribution is nonuniform along the length of the tube. The frictional resistance is the dominant mechanism contributing to bond strength, followed by mechanical interlocking action, whereas the effect of chemical bonding action appears to be limited. The influence of the concrete strength on the interfacial bond strength of the CFSTs was not obvious. The test results of a study by Jianbin et al. [18] and Nardin and El Debs [19] show that the longitudinal strain of a steel tube is exponentially distributed along the length direction. With the increase of the width-to-thickness ratio, the bond strength decreases, and the bond strength does not change with the increase of the slenderness ratio. The shear connectors are very efficient to decrease the bond-slip and increase the maximum load capacity. Liu [20] discovers through experimental studies that the strength of core concrete has no obvious influence on the bond strength of CFSTs. The roughness of the inner surface of a steel tube has a significant influence on the bond strength.

In summary, the test results of the bond-slip performance of CFSTs are more discrete, the influencing factors are complex and diverse, and the previous research results are not the same. In this paper, the influence of the concrete strength, the slenderness ratio, the width-to-thickness ratio, and the presence of rust in the inner wall of the square steel tube on the bond-slip performance of CFSSTs is investigated, and 10 CFSST specimens are utilized for push-out tests. Using orthogonal experimental design, without considering the interaction between the various factors, a total of 9 specimens (CFST1–CFST9) were designed. In addition, in order to study the influence of the internal surface of the steel tube on the bond-slip performance of CFSSTs, a specimen (CFST10) was designed and compared with the CFST4 specimen. The mechanism of the bond-slip and the distribution law of the interfacial bond strength of the CFSSTs under an ultimate bond load are studied. The influence of various factors on the bond strength is analyzed. The influence trend and influence efficiency of various influencing factors on the bond slip performance of concrete-filled steel tubes provide important guidance for the design and construction of concrete-filled steel tubular structures. A theoretical formula for the relative slip of CFSSTs is deduced, which has important theoretical significance and practical value in engineering for improving the design theory of CFSTs [21].

2. Experimental Study

2.1. Specimen Design. The influence of the concrete strength (f_{cu}), the slenderness ratio (λ), and the width-to-thickness ratio (β) on the bond-slip performance of CFSSTs is considered. The detailed parameters of each specimen are shown in Table 1.

The square steel tube used in the test was welded with four steel plates. Acted as the loading end of the specimens, one end of the steel tube was spot-welded together with a 2 mm thick square steel plate whose dimensions were slightly larger than those of the square steel tube. The other end of the steel tube acted as the free end of the specimen. In addition to CFST10, the inner walls of the other specimens were treated with manual derusting. According to the Chinese standard GB/T 8923.1-2011 [22], using the electric grinder on steel tube inner surface derusting, the inner surface of the steel tube after the derusting is closest to the standard model photo, and the derusting is qualified. The internal corrosion grade of the CFST10 specimen steel tube was B grade, and the manual derusting grade of the other specimens was ST2. The loading ends of the test specimens were placed on flat level ground, and the core concrete was poured into the free end of the specimen. A vibrating bar was used to pack the concrete tightly. The concrete was poured to the specimens' free end (50 mm). Then, the concrete was screeded, leaving an empty steel tube that was 50 mm long. At the same time, 3 sets of test concrete cubes ($100 \times 100 \times 100$ mm) were reserved as the core concrete specimens of each strength grade. The reserved test concrete cubes and specimens were cured under the same conditions. The core concrete surface was covered with a plastic wrap after the final solidification of the concrete. It was watered regularly to ensure moist curing and to better simulate the curing environment of the construction site.

To avoid local buckling in the steel tube due to the stress concentration at the end of the steel tubes, several stiffeners ($150 \times 50 \times 4$ mm) were welded on the outer surface of the free end of the specimens, as shown in Figures 1 and 2. When the specimens were processed, a longitudinal notch was arranged at the same horizontal positions of the two intersecting steel tube walls on each square steel tube. Before the initial solidification of the core concrete, the steel strips ($200 \times 20 \times 2$ mm) were inserted horizontally from the longitudinal notch. The resistance strain gauges were arranged at the same horizontal position of the two other steel tube walls without longitudinal notches, as shown in Figures 1–3.

2.2. Material Performance Test. The yield stress of the steel used during the tests was 235 MPa. According to the Chinese code GB/T 228.1-2010 [23], the test results of the steels with different thicknesses are shown in Table 2.

The core concrete was made of ordinary portland cement (P.O. 42.5) produced by the Qingdao branch of Shandong

Table 1: Design parameters of the test specimens.

Specimen number	L (mm)	$f_{cu,0}$ (mm)	B (mm)	$\lambda = 2\sqrt{3}L/B$	$\beta = B/t$	$f_{cu,0}$ (MPa)	Inner wall of the steel tube
CFST1	400.00	5.00	150	9.24	30.00	30.00	Rust cleaning
CFST2	400.00	4.00	150	9.24	37.50	40.00	Rust cleaning
CFST3	400.00	3.00	150	9.24	50.00	50.00	Rust cleaning
CFST4	600.00	5.00	150	13.86	30.00	40.00	Rust cleaning
CFST5	600.00	4.00	150	13.86	37.50	50.00	Rust cleaning
CFST6	600.00	3.00	150	13.86	50.00	30.00	Rust cleaning
CFST7	800.00	5.00	150	18.48	30.00	50.00	Rust cleaning
CFST8	800.00	4.00	150	18.48	37.50	30.00	Rust cleaning
CFST9	800.00	3.00	150	18.48	50.00	40.00	Rust cleaning
CFST10	600.00	5.00	150	13.86	30.00	40.00	No rust removal

Note. L is the steel tube length, B is the steel tube section width, t is the steel tube thickness, and $f_{cu,0}$ is the concrete strength.

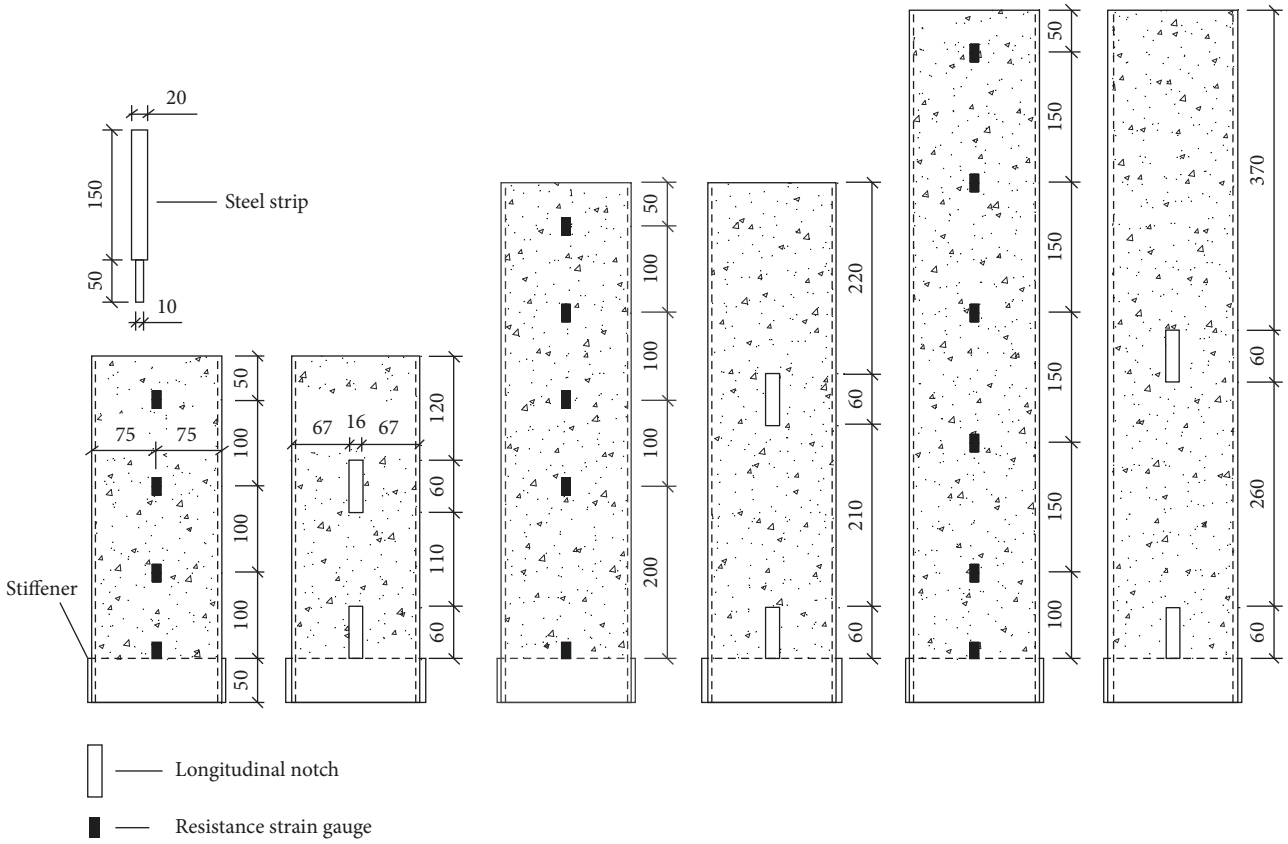

Figure 1: Distribution of steel strips, resistance strain gauges, and longitudinal notches (mm).

Shanshui Cement Group Limited. According to the Chinese code JGJ55-2011 [24], 3 strength grades (30 MPa, 40 MPa, and 50 MPa) of concrete were prepared. According to the Chinese code GB/T 50081-2002 [25], the concrete cubes reserved for the different strength grades were cured for 28 days. The material consumption and the test results of the mechanical properties of concrete are shown in Table 3.

2.3. Loading Device and Loading Scheme. The tests were carried out in the Shandong Provincial Key Laboratory of Civil Engineering Disaster Prevention and Mitigation. After all the specimens were cured for 28 days, the square steel plates at the loading ends of the specimens were cut off, and the push-out tests were carried out in turn. The loading device diagram is shown in Figure 4. Before testing, the ends of the specimens were mechanically polished, and a layer of sand was placed on the steel backing plate at the bottom of the specimens. Then, the free ends of the specimens were placed on the sand. The loading ends of the test specimens were fixed with a loading head that was welded using a steel cushion block ($130 \times 130 \times 60$ mm) and a steel backing plate ($200 \times 200 \times 20$ mm), as shown in Figures 2 and 4. The upper part of the loading head is a 50 t hydraulic jack, and the upper part of the jack is equipped with a pressure sensor. Several displacement meters were attached to an

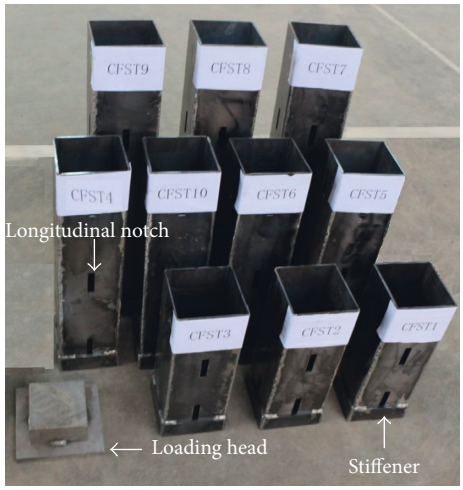

Figure 2: Square steel tubes.

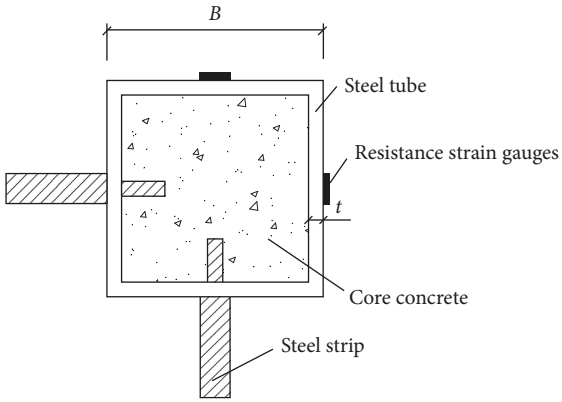

Figure 3: Cross-sectional area of specimens.

independent bracket to measure the displacements at different locations of the specimens, as shown in Figure 4. The test data were recorded using the static data acquisition system. The actual loading picture in the test is shown in Figure 5.

The tests were conducted by preloading with 2 kN without recording data so that each test component was squeezed tightly. Each test part was checked and corrected to ensure that the instrument was normal. During the initial stage of loading, each stage load was approximately 1/10 of the predicted ultimate bond load of each specimen. When loaded to the predicted limit load of 1/2, each stage load was 2 kN, and the control loading speed was 200 N/s. Each stage load lasted 1 minute. When obvious nonlinear slip between the steel tube and the core concrete was observed, the loading speed was controlled slowly and continuously to 500 N/s until the core concrete slipping reached 40 mm. The loading scheme of all specimens was the same, and when the core concrete slippage reached 40 mm, the test was stopped.

2.4. Measurement Scheme. The relative slip between the square steel tube and the core concrete was measured using the steel strip extracted from the slotted steel tube and the displacement meter attached to the independent bracket. The measured values of the two displacement meters at the same horizontal position on the two vertical intersecting steel tube walls were averaged to provide the final test data at the horizontal position, as shown in Figures 3 and 4. After processing the data of the displacement meter at the different positions, the relative slip distribution curve of the core concrete along the specimen height direction was obtained.

The thickness of the steel tube wall was much smaller than its length. The strain on the outer surface of the steel tube was approximately equal to the strain on the inner surface of the steel tube. This relation enabled convenient strain measurements and did not affect the interfacial bond effect between the core concrete and square steel tube. The measured values of the strain gauges at the same horizontal position on the other two vertical intersecting steel tube walls were averaged and treated as the strain value at the horizontal position, as shown in Figures 3 and 4. The distribution curve of the longitudinal strain of the square steel tube with the change in the load was obtained by processing the test data of the strain gauges at the different positions. Moreover, the distribution laws of the bond stresses along the specimen height could also be obtained by further calculations and analyses.

Table 2: Mechanical properties of the steel.

x	δ (%)	f_y (kN)	f_u (kN)	E_s (MPa)
5.00 mm	23.80	92.10	123.10	2.06×10^5
4.00 mm	27.25	71.75	95.35	2.04×10^5
3.00 mm	28.80	74.85	98.45	1.91×10^5

3. Test Result and Analysis

3.1. Test Phenomenon. During the early stages of loading, the readings of the specimens from the displacement meters were almost unchanged. With the increase in the load, the displacement meter readings at the loading end of the specimens increased greatly. Then, the readings of the displacement meters in the middle of the specimens and the free ends slowly increased, and the displacement meters' reading at the loading ends of the specimens became relatively large. As the load continued to increase, the specimens produced a "snap" sound, and significant interface slipping occurred at the core concrete of the loading ends of the specimens. The displacement meter increments at the loading ends and the free ends of the specimens were basically consistent, and the core concrete began to slip evenly as a whole. At this point, the load of some specimens had a slow growth trend, but all specimens were on the decline.

By carefully observing the specimens after the tests, all the specimens of the square steel tube did not exhibit the buckling phenomenon, and the specimen loading ends and free ends of the core concrete did not exhibit obvious cracking. A small amount of concrete debris was produced at the loading ends of the specimens. It is clear that the core

Table 3: Material consumption and mechanical properties of concrete.

Concrete strength grade (MPa)	Material consumption (kg/m^3)				Water/cement ratio	f_{cu} (MPa)	E_c (MPa)
	Water	Cement	Sand	Gravel			
30.00	184.00	385.00	775.00	1050.00	0.48	34.11	3.11×10^4
40.00	183.00	460.00	730.00	1065.00	0.40	42.18	3.31×10^4
50.00	180.00	515.00	700.00	1080.00	0.35	51.88	3.48×10^4

Note. E_c is the elastic modulus of the concrete, and f_{cu} is the compressive strength of the concrete cube.

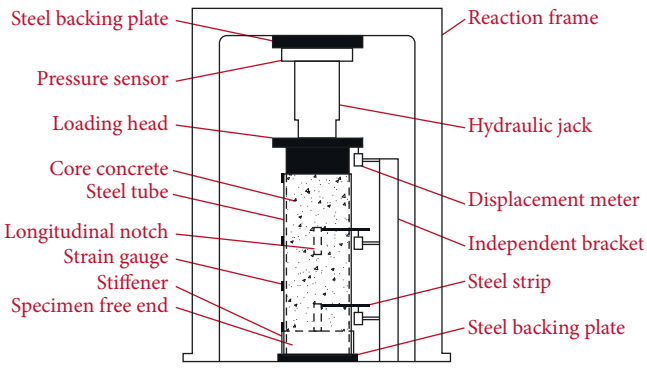

Figure 4: Details of test setup.

Figure 5: Actual loading picture.

concrete was pushed out with traces of the steel tubes, and interface bond force failure occurred, as shown in Figure 6.

3.2. Load-Slip Curves. After the push-out tests, the loading end and free end displacement data of the specimens were introduced into Origin software for analysis and processing. The loading end and free end load-slip curves (P-S curves) of the specimens were obtained and are shown in Figures 7 and 8.

By comparing Figures 7 and 8, it is shown that the load-slip curve at the loading end of the same specimen is nearly the same as the free end load-slip curve. The development of

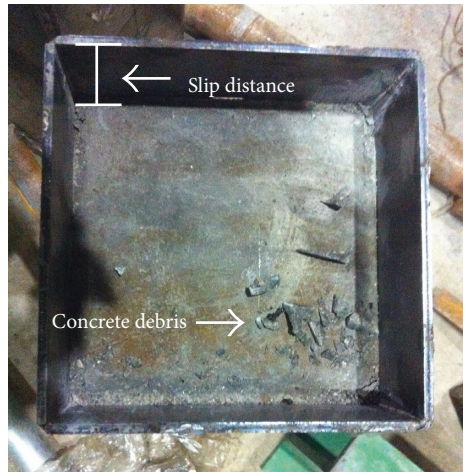

Figure 6: Failure mode of CFST4 specimen.

relative slip at the loading ends occurred earlier than that at the free ends. At the initial stage of loading, the slippage of the interface between the steel tube and the core concrete was very small. When the load (P) increased to approximately 25% of the value of the ultimate bond load (P_u), the interface of the CFSST began to slip clearly. When the ultimate bond load (P_u) is approached, two different cases can be seen in the load-slip curves. One is that the load-slip curves have no peak point, but at the inflection point of the curves, the curvature have changed obviously, and then, the curves show a steady upward trend, such as the load-slip curves of CFST1–CFST4 in Figures 7 and 8. The other is that the curves show a downward trend after the peak point of the load-slip curves, and the slip develops rapidly, and then, the curves show a gentle upward trend, such as the load-slip curves of CFST5–CFST9 in Figures 7 and 8. The peak point or inflection point is the ultimate bond load of the CFST specimens [26]. When relative slip occurred between the steel tube and core concrete throughout the whole length of the interface, the chemical bonding action of the whole interface stopped working. At this time, the interface of the mechanical interlocking action and frictional resistance of the whole interface also changed. The composition and size of the interfacial bond force were different when the load exceeded the ultimate bond load. When the chemical bonding action, mechanical interlocking action, and frictional resistance along the entire interface prior to bond failure were greater than the sum of the mechanical interlocking action and frictional resistance after the bond failure of the entire interface, the load-slip curve exhibits a clear peak point and a subsequent downward trend.

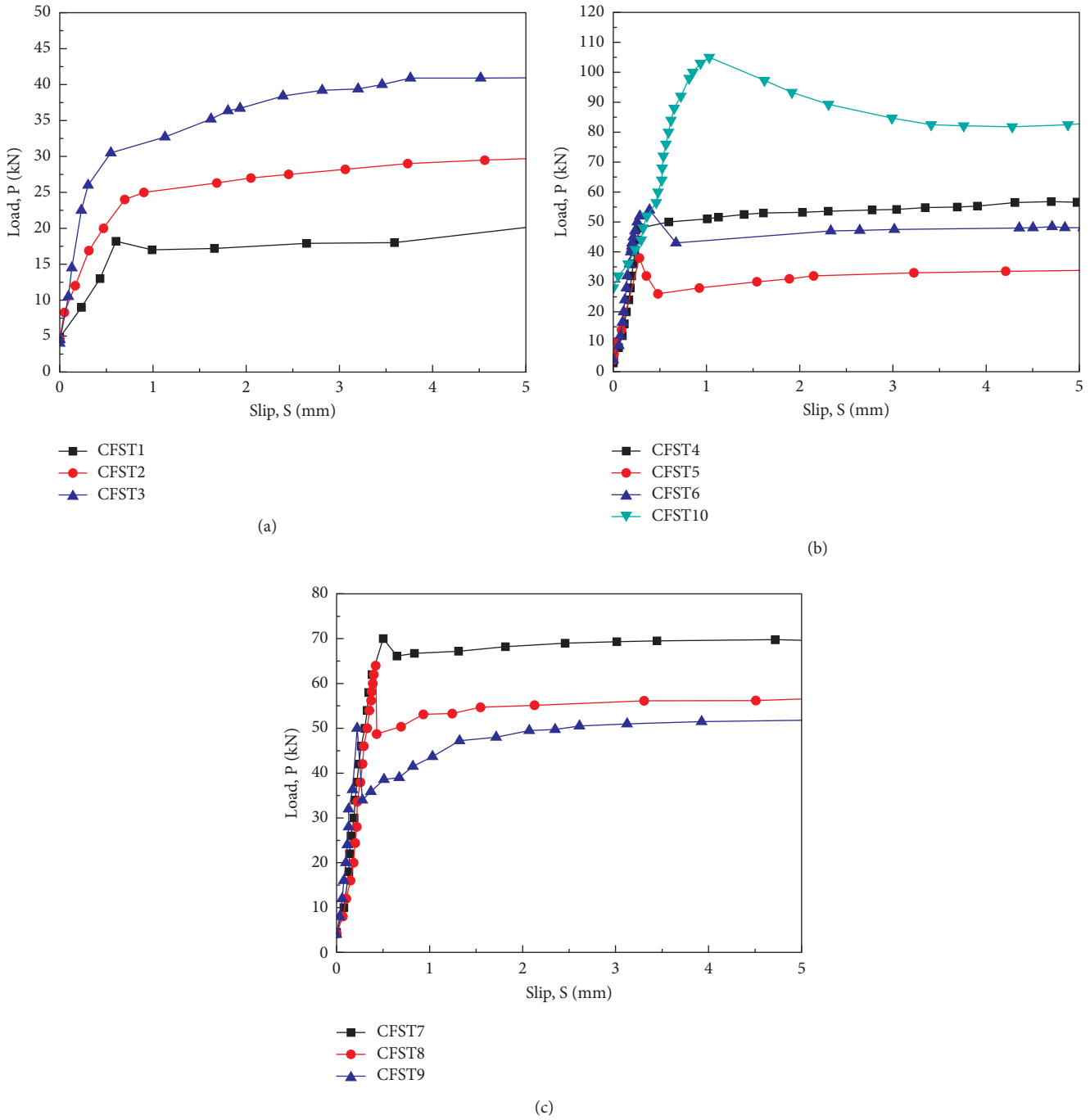

Figure 7: P-S curves of the loading ends.

Otherwise, the load-slip curve exhibits an obvious inflection point and a subsequent upward trend.

With the increase in the specimen length, the load-slip curve of the specimens gradually changed from the inflection point to the obvious peak point, and the ultimate bond load gradually increased. Before the specimens reached the ultimate bond load, the load-slip curves were basically linear, and the slip was relatively small. When the load exceeded the ultimate load, the curves exhibited a nonlinear change, and the speed of the slip was faster. At this time, the interface slip between the steel tube and the core concrete was very large. Therefore, in practical engineering, the law of the load-slip curve variation after reaching the ultimate bond load is not very important.

3.3. Strain along the Longitudinal Distribution of the Specimens. Figure 9 is the longitudinal strain distribution curve of the square steel tube for some specimens before reaching the ultimate bond load. The variable x in Figure 9 represents the distance from the free end of the specimens, and $\varepsilon_s(x)$ represents the longitudinal strain of the steel tubes.

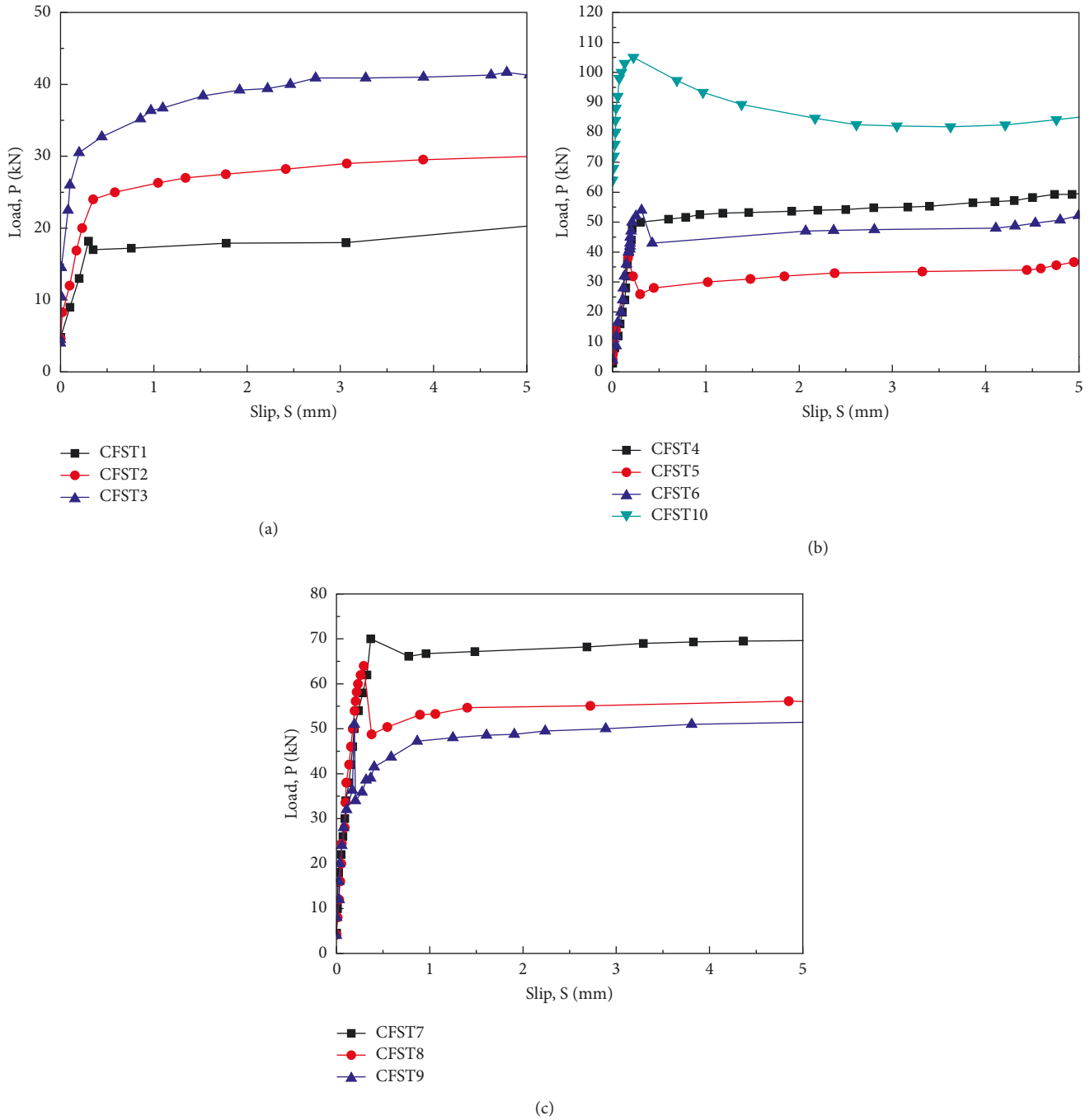

Figure 8: P-S curves of the free ends.

As shown in Figure 9, the longitudinal strain of the steel tube increased with the increase of the load. The longitudinal strain of the steel tube decreased gradually from the free end to the loading end of the specimens. At the free end of the specimens, the steel tube strain grew more quickly than that at the loading end. With the increase of the load, the steel tube strain along the interface length exhibited an overall negative exponential distribution. The strain rate in the middle of the steel tube became larger, and the strain increased rapidly. Therefore, the steel tube strain curves gradually exhibited a convex trend from a lower concave trend. This analysis argues that the load of the core concrete at the loading end of the specimens was transferred to the steel tube through a certain bond length. At the same time, the load at the free end of the steel tube was transferred to the core concrete through a certain length of the interfacial bond force. The interface between the two ends of the specimen began to slip at first, and the chemical bonding action was destroyed. As the load continued to increase, the bond force at the interface of the specimens gradually broke at

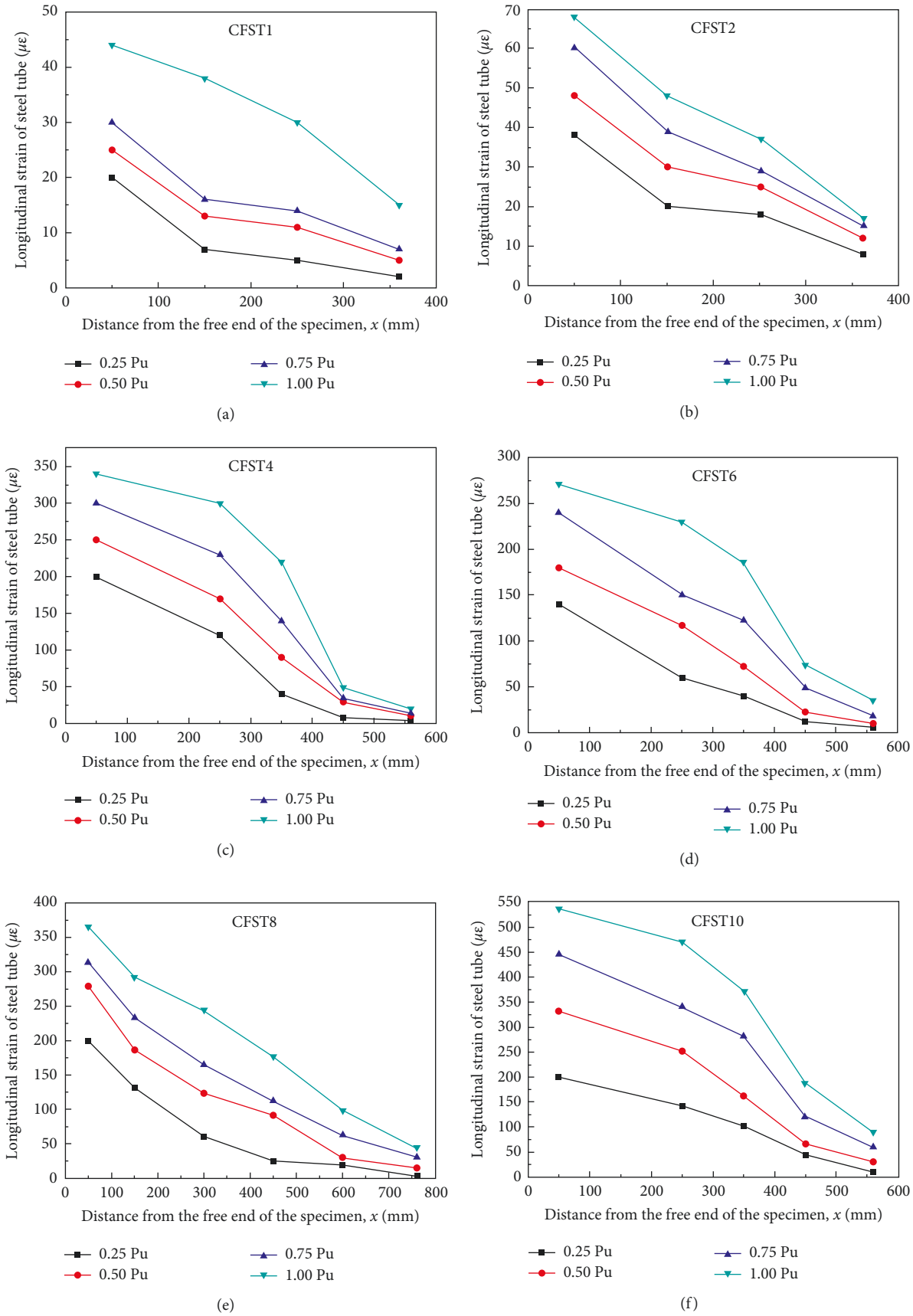

Figure 9: Longitudinal strain of steel tubes.

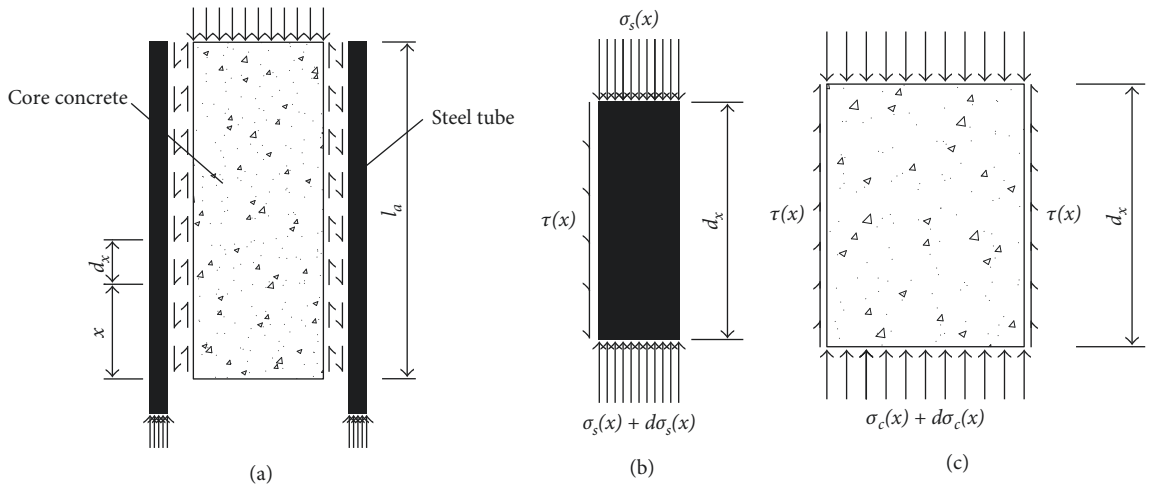

Figure 10: Stress analysis of the CFSSTs: (a) interaction between the steel tube and the core concrete; (b) equilibrium of a small element of the steel tube and (c) the core concrete.

the two ends towards the middle. At this time, the bonding force between the steel tube and core concrete was mainly composed of the frictional resistance and mechanical interlocking action on the relative slip interface, the frictional resistance, the mechanical interlocking action, and the chemical bonding force on the interface without relative slip in the middle of the specimens. Therefore, the strain in the steel tube in the middle of the specimen increased rapidly until relative slip occurred along the whole interface length.

The test results also show that the strain value of the steel tubes was not large from the beginning load to the ultimate bond load. When the maximum strain was reached, the steel tube did not yield. The steel tube was in an elastic state throughout the test. Through the statistical analysis and fitting of the strain data under each stage load, it was reasonable to fit the distribution curve of the steel tube strain along the length of the steel tube using the exponential in

$$\begin{aligned}
\varepsilon_s(x) &= A_1 e^{(-x/t_1)} + y_0,\\
A_1 &= -2111.52020\left(\frac{P}{P_u}\right) + 12.7039 \times 2\sqrt{3}\left(\frac{L}{B}\right)\\
&\quad - 1.8366\left(\frac{B}{t}\right) + 5.7317 f_{\mathrm{cu}},\\
t_1 &= -52789.4248\left(\frac{P}{P_u}\right) + 13.0654 \times 2\sqrt{3}\left(\frac{L}{B}\right)\\
&\quad +0.0104\left(\frac{B}{t}\right) + 256.9209 f_{\mathrm{cu}}.
\end{aligned} \tag{1}$$

3.4. Average Bond Strength. When specimen bond failure occurred, the whole interface exhibited bond failure. At this point, the ultimate bond load (P_u) corresponding to the load-slip (P-S) curve could be considered as the ultimate bond force at the entire interface. Therefore, the average bond strength was calculated using the following formula [14, 26]:

$$\overline{\tau} = \frac{P_u}{A}, \tag{2}$$

where A is the contact area between the inner wall of the steel tube and the core concrete; $A = 4(B-2t)l_a$, where l_a is the interface length of the bond stress between the steel tube and the core concrete.

3.5. Bond Stress Distribution along the Specimen Height. The stress diagrams of the CFSST specimen and the infinitesimal body of the steel tube and the core concrete are shown in Figure 10, and the equilibrium equations can be obtained as follows:

$$\tau(x)(B-2t) = (B-t)t\frac{d\sigma_s(x)}{dx}, \tag{3}$$

$$A_s d\sigma_s(x) + A_c d\sigma_c(x) = 0, \tag{4}$$

where $\tau(x)$ is the bond stress between the steel tube and the core concrete interface; B is the section width of the steel tube; t is the steel tube thickness; $\sigma_s(x)$ is the axial compressive stress acting on the steel tube; $\sigma_c(x)$ is the axial compressive stress acting on the core concrete; and A_c is the core concrete cross section area.

Equation (3) can be simplified as

$$\tau(x) = E_s t\frac{d\varepsilon_s(x)}{dx}, \tag{5}$$

where E_s is the elastic modulus of the steel tube and $\varepsilon_s(x)$ is the longitudinal strain of the steel tube.

Using (1) and (5), we obtain

$$\tau(x) = -E_s t\frac{A_1}{t_1}e^{(-x/t_1)}. \tag{6}$$

The bond stress distribution curves for 25% P_u, 50% P_u, 75% P_u, and 100% P_u corresponding to the specimens were obtained using (6), and the stress distribution curves of some specimens are shown in Figure 11.

From Figure 11, it can be seen that the bond stress between the loading ends and free ends increases gradually as the load increases, before the load reaches the ultimate bond

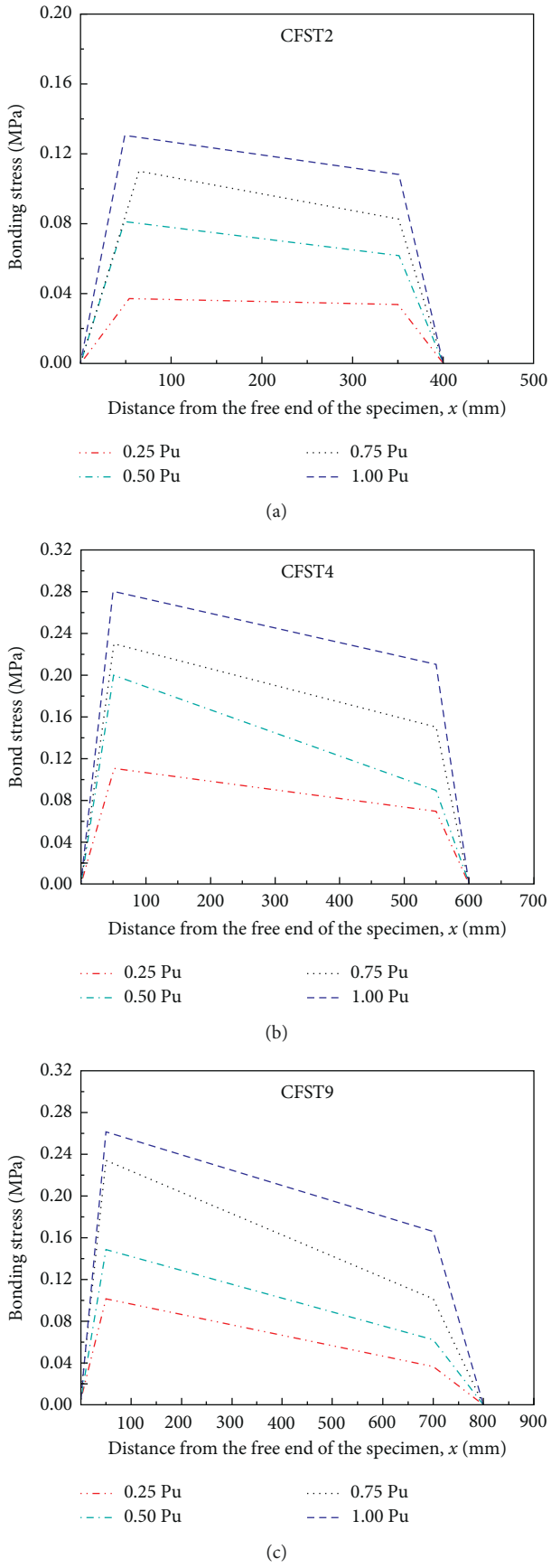

Figure 11: Distribution of bond stresses: (a) CFST2; (b) CFST4; (c) CFST9.

load. The interfacial bond stress at the loading end of the specimens was smaller than the interfacial bond stress at the free end of the specimens. The difference in the bond stress between the loading ends and free ends increased gradually. The analysis shows that the core concrete of loading ends and the steel tube of free ends withstood the same load at the same time, but the deformation properties of the core concrete and steel tube were different. When the same load was applied, the interface length required at the loading end of the specimen was longer than that at the free end of the specimen. Therefore, the strain in the steel tube at the loading end of the specimens and the interfacial bond stress were smaller.

3.6. Calculation and Analysis of Bond-Slip. According to the force analysis of the specimen shown in Figure 10, the coordinate relation between the steel tube and core concrete shows that the relative slip is $S(x)$ when the free end of the distance specimen is x (mm).

$$S(x) = \int [\varepsilon_c(x) - \varepsilon_s(x)]dx, \tag{7}$$

where $\varepsilon_c(x)$ is the core concrete longitudinal strain.

Using (4), we obtain the following:

$$\varepsilon_c(x) = -\frac{A_s E_s}{A_c E_c}\varepsilon_s(x). \tag{8}$$

Assigning $k = A_s E_s / A_c E_c$ and substituting (8) into (7), the following derivative can be obtained:

$$\frac{d^2 S(x)}{dx^2} = -(1+k)\frac{d\varepsilon_s(x)}{dx}. \tag{9}$$

Then, (5) is substituted into (9) and the integral is calculated:

$$S(x) = \frac{1+k}{E_s t} \cdot A_1 \cdot t_1 \cdot e^{(-x/t_1)} + C_1 x + C_2. \tag{10}$$

Equation (10) should satisfy the following two boundary conditions: (1) the relative slip of the interface at the free end of the specimens ($x = 0$) is the deformation of the hollow steel tube at the free end: $S(0) = S_0$; (2) after a certain range of interfacial bond-slip ($x = l_b$), the strain of the steel tube is the same as that of the core concrete, and the relative slip is 0: $S(l_b) = 0$, where S_0 is the relative slip between the steel tube and the core concrete of free ends. The free ends of the specimens were welded with stiffeners on the outside. According to Figure 9, $S_0 = P/E_s' A_s'$, where E_s' and A_s' are the elastic modulus and the cross-sectional area of the hollow steel tube with free ends of specimens and l_b is the interfacial shear transfer length when the strain of the steel tube is the same as that of the core concrete. Then, $u\int_0^{l_b} \tau(x)\,dx = P$ can be solved as follows: $l_b = -t_1 \ln((P/uE_s t A_1) + 1)$, where P is the load on the specimens and u is the perimeter of the inner wall of the steel tube.

From the above two boundary conditions, the following can be obtained:

Table 4: Experimental results and corresponding range analysis.

Specimen number	Influence factor			P_u (kN)	$\overline{\tau}$ (MPa)
	λ	β	$f_{cu,0}$ (MPa)		
CFST1	9.24	30	30	19.32	0.0986
CFST2	9.24	37.5	40	26.39	0.1327
CFST3	9.24	50	50	32.57	0.1616
CFST4	13.86	30	40	49.59	0.1610
CFST5	13.86	37.5	50	39.82	0.1275
CFST6	13.86	50	30	53.27	0.1682
CFST7	18.48	30	50	72.18	0.1719
CFST8	18.48	37.5	30	65.48	0.1537
CFST9	18.48	50	40	50.36	0.1166
P_u					
I_j	78.28	141.09	138.07		
II_j	142.68	131.69	126.34	$T = 514.85$	—
III_j	188.02	136.20	144.57		
R_j	109.74	9.40	18.23		
$\overline{\tau}$					
I_j	0.3929	0.4315	0.4205		
II_j	0.4567	0.4139	0.4103	—	$T = 1.0535$
III_j	0.4422	0.4464	0.4610		
R_j	0.0638	0.0325	0.0507		
CFST10	13.86	30	C40	105.87	0.3437

Note. I, II, and III represent the various factor values (levels) ranging from small (low) to large (high); j represents various factors, R_j represents the range of the data, and T stands for the sum of the data. For example, I_j represents the sum of the values of the test parameters corresponding to level "1" of the influence factors in the column "j".

$$C_1 = \frac{(1+k)P}{E_s^2 t^2 u \ln\left((P/uE_s tA_1)+1\right)} + \frac{P}{E_s' A_s' t_1 u \ln\left((P/uE_s tA_1)+1\right)},$$

$$C_2 = \frac{P}{E_s' A_s'} - \frac{1+k}{E_s t} A_1 t_1. \tag{11}$$

After substituting C_1 and C_2 into (10), the theoretical formula of the relative slip of the interface of the CFSST push-out tests can be obtained.

4. Analysis of the Influencing Factors

Through the analysis and calculations of the push-out test data, the ultimate bond load (P_u) and the average bond strength ($\overline{\tau}$) of the specimens can be obtained, and the test data of specimens CFST1–CFST9 were processed using orthogonal experiment and extremum difference analysis methods, as shown in Table 4.

As shown in Table 4, the ranges of $R_j = \max\{I_j, II_j, III_j\} - \min\{I_j, II_j, III_j\}$ for the various factors are different. Hence, the test results were affected by the different values of the different factors. The greater the range was, the greater the influence of the factor to the test indexes was. Therefore, it can be seen in Table 4 that the most significant influence factor that affected the bond-slip performance of the CFSST was the presence of rust on the inner wall of the steel tube. The influence of the other factors decreased in the following order: the slenderness ratio (λ), the concrete strength (f_{cu}), and the width-to-thickness ratio (β).

4.1. Influence of the Slenderness Ratio. According to the test data in Table 4, the ultimate bond load increased with the increase in the slenderness ratio; the average bond strength increased first and then decreased with the increase in the slenderness. When the slenderness ratio was 13.86, the average bond strength reached the peak point. From the analysis, we found that there is a limit value for the average bond strength of the interface of a definite cross section of the CFSST. With the increase of the load, the relative slip between the steel tube and the core concrete occurred within a certain range of the two ends of the specimens, and the load transfer efficiency on the interface was weakened. The reason for this phenomenon is that the cross section size of the specimen is the same, and the longer the slenderness ratio is, the longer the specimen length is. The longer the length of the specimen, the greater the contact area between the core concrete and the inner surface of the steel tube, so the ultimate bond load of the specimens was greater. The load of the core concrete at the loading ends and the load of the steel tube at the free ends were the same, and the load at the two ends of the specimens had caused a certain damage to the interfacial bond force along the length direction of the specimens. The larger the load is, the larger the range of interfacial bond failure at both ends of the specimen is. Therefore, the average bond force of specimens had a peak point with the increase of the slenderness ratio. In addition, when the load was too high, the steel tube reached the yield strength earlier, reducing the interfacial bond stress between the tube and the core concrete.

4.2. Influence of the Concrete Strength. From Table 4, it can be seen that the strength of the concrete influenced the average bond strength and ultimate bond load of the specimens. When the core concrete strength grade was below 40 MPa, the average bond strength and ultimate bond load decreased with the increase in the concrete strength grade. When the strength grade of the core concrete was above 40 MPa, the average bond strength and ultimate bond load increased with the increase of the core concrete strength grade. This test result is consistent with the experimental results of Lihong and Shaohuai [12, 13] and Lihua et al. [27]. The analysis shows that when the concrete strength grade was below 40 MPa, the interfacial bond force between the concrete and steel tube cannot resist the influence of shrinkage of concrete setting and hardening. At this time, the shrinkage of core concrete played a dominant role in the interfacial bond force. When the concrete strength grade was above 40 MPa, the increase of the core concrete strength increased the interfacial bond force, which was greater than the adverse effect of concrete shrinkage on the interfacial bond force.

4.3. Effect of the Specimen Width-to-Thickness Ratio. Table 4 shows that the average bond strength and ultimate bond

strength first decreased and then increased with the increase of the width-to-thickness ratio. The changes were small relative to the other factors. When the width-to-thickness ratio was 37.5, the average bond strength reached a minimum value. The analysis shows that the cross section size of the specimens was the same, and the thickness of the steel tube was larger when the specimen thickness was relatively small, which had a greater restraint force on the transverse deformation of the core concrete at the loading ends under the vertical pressure. The mechanical interlocking action and the frictional resistance were increased, and the interfacial bond force was increased. The transfer efficiency of the interfacial bond force on the free ends was higher. With the increase of the width-to-thickness ratio of the specimen, the area of the contact area between the steel tube and the core concrete increased, and the average bond strength and ultimate bond strength of the specimen increase slowly.

4.4. The Presence of Rust on the Inner Surface of the Steel Tube. It can be seen from Table 4 that the presence of rust on the inner wall of the steel tubes had an important influence on the bond-slip performance of the CFSST. Under the same conditions, the ultimate bond load and average bond strength of the specimens with rust on the inner wall of the steel tube were more than double compared to those of the specimens with the rust removed. This is because the corrosion grade of the inner wall of the steel tube was B, which enhanced the chemical bonding action, mechanical interlocking action, and frictional resistance at the interface between the steel tube and core concrete.

5. Conclusion

Based on the experimental study of 10 CFSST specimens, the following conclusions were obtained:

(1) The load-slip curves at the two ends of the same specimen were approximately the same, and the bond failure and relative slip of the interface of the specimens gradually developed from the two ends towards the middle of the specimens.

(2) The strain of the steel tube exhibited a negative exponential distribution along the length of the interface. With the increase in the load, the bond stress in the middle of the specimen increased gradually, and the concave steel tube strain curve gradually presented a convex trend during the test.

(3) The interfacial bond stress at the loading end of the specimens was smaller than that at the free end of the specimens. When the specimen reached the ultimate bond load, the entire core concrete slipped rapidly, and the slip was large. This phenomenon should be considered during practical engineering applications.

(4) The order of these influence factors from main to secondary was the presence of rust in the inner wall of the square steel tube, the slenderness ratio, the core concrete strength, and the width-to-thickness ratio. When the corrosion grade of the steel tube is B, the interfacial bond strength of the CFSST can be doubled.

Conflicts of Interest

The authors declare that they have no conflicts of interest regarding the publication of this paper.

Acknowledgments

This study was financially supported by the Project of Science and Technology Innovation Fund for graduate students of the Shandong University of Science and Technology (no. YC150215).

References

[1] H. Linhai and Y. Youfu, *Modern Concrete Filled Steel Tubular Structures*, pp. 263–269, China Building Industry Press, Beijing, China, 2nd edition, 2007.

[2] S. Morino and K. Tsuda, "Design and construction of concrete-filled steel tube column system in Japan," *Earthquake Engineering and Engineering Seismology*, vol. 4, no. 1, pp. 51–73, 2003.

[3] C. Lihua, D. Jixiang, L. Yu, and L. Shuting, "Review analysis on study of bond behavior of concrete-filled steel tube," *Building Structure*, vol. 46, no. 22, pp. 78–83, 2016.

[4] K. Xiliang, C. Yao-fang, Z. Li, and Z. Hong-tie, "Theoretical analysis of bond-slip constitutive ralationship for CFST," *Engineering Mechanics*, vol. 26, no. 10, pp. 74–78, 2009.

[5] C. Xu, H. Chengkui, J. Decheng, and S. Yuancheng, "Push-out test of pre-stressing concrete filled circular steel tube columns by means of expansive cement," *Construction and Building Materials*, vol. 23, no. 1, pp. 491–497, 2009.

[6] H. Shakir-Khalil, "Push-out strength of concrete-filled steel hollow sections," *Structural Engineer*, vol. 71, no. 13, pp. 230–233, 1993.

[7] R. Abendeh, H. S. Ahmad, and Y. M. Hunaiti, "Experimental studies on the behavior of concrete-filled steel tubes incorporating crumb rubber," *Journal of Constructional Steel Research*, vol. 122, pp. 251–260, 2016.

[8] K. Xiliang, Z. Hongtie, and X. Jianyang, "Summary and analysis of bond slip of concrete filled steel tube," *Journal of Xi'an University of Architecture and Technology*, vol. 38, no. 3, pp. 321–326, 2006.

[9] Z. Tao, L.-H. Han, B. Uy, and X. Chen, "Post-fire bond between the steel tube and concrete in concrete-filled steel tubular columns," *Journal of Constructional Steel Research*, vol. 67, no. 3, pp. 484–496, 2011.

[10] K. S. Virdi and P. J. Dowling, "Bond strength in concrete filled circular steel tubes," in *CESLIC Report CC11*, Department of Civil Engineering, Imperial College, London, UK, 1975.

[11] K. S. Virdi and P. J. Dowling, "Bond strength in concrete filled steel tubes," *IABSE Proceeding*, vol. 3, pp. 125–139, 1980.

[12] X. Lihong and C. Shaohuai, "Bond strength of composite interface of concrete filled steel tubular column (top)," *Building Science*, vol. 12, no. 3, pp. 22–28, 1996.

[13] X. Lihong and C. Shaohuai, "Bond strength of composite interface of concrete-filled steel tube column: (under)," *Building Science*, vol. 12, no. 4, pp. 19–23, 1996.

[14] X. S. Qu, Z. H. Chen, D. A. Nethercot, L. Gardner, and M. Theofanous, "Push-out tests and bond strength of rectangular CFST columns," *Steel and Composite Structures*, vol. 19, no. 1, pp. 21–41, 2015.

[15] Q. Xiushu, C. Zhihua, and D. A. Nethercot, "Load-reversed push-out tests on rectangular CFST columns," *Journal of Constructional Steel Research*, vol. 81, pp. 35–43, 2013.

[16] L. Yongjian and C. Jianjun, "Push-out test on shear bond strength of CFST," *Industrial Construction*, vol. 36, no. 4, pp. 78–80, 2006.

[17] Y. Chen, R. Feng, Y. B. Shao, and X. T. Zhang, "Bond-slip behaviour of concrete-filled stainless steel circular hollow section tubes," *Journal of Constructional Steel Research*, vol. 130, pp. 248–263, 2017.

[18] W. Jianbin, X. Jianyang, Z. Hongtie, and T. Ximing, "Experimental study on bond-slip behavior between steel and concrete in square concrete filled steel structures," *Building Structure*, vol. 37, no. 10, pp. 74–77, 2007.

[19] S. D. Nardin and A. L. H. C. El Debs, "Shear transfer mechanisms in composite columns:an experimental study," *Steel and Composite Structures*, vol. 7, no. 5, pp. 377–390, 2007.

[20] Z. Y. Liu, "Experiment study on interfacial normal bond strength of concrete filled steel tube," *Advanced Materials Research*, vol. 594–597, pp. 947–954, 2012.

[21] L. Yong-jian, L. Jun-ping, G. Yong-ping, and C. Jian-jun, "Bond-slip mechanics behaviors of structures concrete filled steel tubes," *Journal of Chang'an University*, vol. 27, no. 2, pp. 53–57, 2007.

[22] National Standards of the People's Republic of China, *Preparation of Steel Substrates before Application of Paints and Related Products-Visual Assessment of Surface Cleanliness-Part 1: Rust Grades and Preparation Grades of Uncoated Steel Substrates and of Steel Substrates after Overall Removal of Previous Coatings, GB/T 8923.1-2011*, Standards Press of China, Beijing, China, 2011.

[23] National Standards of the People's Republic of China, *Metallic Materials-Tensile Testing-Part 1: Method of Test at Room Temperature, GB/T 228.1-2010*, Standards Press of China, Beijing, China, 2010.

[24] Profession Standard of the People's Republic of China, *Specification for Mix Proportion Design of Ordinary Concrete, JGJ 55-2011*, China Architecture & Building Press, Beijing, China, 2011.

[25] National Standards of the People's Republic of China, *Standard for Test Method of Mechanical Properties on Ordinary Concrete, GB/T 50081-2002*, China Architecture & Building Press, Beijing, China, 2003.

[26] C. Shaohuai, *Modern Steel Tube Confined Concrete Structures*, pp. 230–251, China Communications Press, Beijing, China, 2007.

[27] C. Lihua, D. Jixiang, and J. Qiliang, "Refining bond–slip constitutive relationship between checkered steel tube and concrete," *Construction and Building Materials*, vol. 79, pp. 153–164, 2015.